RSC Advances

PAPER

View Article Online
View Journal | View Issue

Cite this: *RSC Adv.*, 2015, **5**, 24953

Silver nanowire/polyimide composite transparent electrodes for reliable flexible polymer solar cells operating at high and ultra-low temperature†

Xiaoyang Guo, Xingyuan Liu,* Jinsong Luo, Zhihong Gan, Zhong Meng and Nan Zhang

Received 8th January 2015
Accepted 27th February 2015

DOI: 10.1039/c5ra00403a

www.rsc.org/advances

A high and ultra-low temperature resistant flexible polymer solar cell was produced using a silver nanowire and polyimide composite transparent electrode. The composite transparent electrode exhibited excellent opto-electrical properties and flexibility across a wide temperature range of −150 to 250 °C. It also demonstrated strong adhesion, good abrasion performance, and excellent thermal and chemical stability. The power conversion efficiency of the flexible polymer solar cell based on this film was comparable to the device based on a flexible indium tin oxide electrode, and is quite stable under a wide range of applied temperatures.

Introduction

Polymer solar cells (PSCs) have attracted tremendous interest due to their low cost, easy fabrication, and compatibility with flexible substrates over a large area. In particular, flexible PSCs have promising applications in some emerging areas, such as portable or wearable electronics, synthetic skin, and conformal solar cells for building integration. Currently, one major challenge in developing flexible PSCs is the lack of deformable transparent conductive films (TCFs), which are the cornerstone of flexible PSCs, allowing light to be transmitted with minimal losses while simultaneously transporting charge. Indium tin oxide (ITO) has high transparency and low resistance which is the preferred choice in many PSC devices.[1–3] However, this material is not without shortcomings, with its brittleness and high price preventing its application in low-cost flexible devices.[4–6] This has led to several alternative TCFs being introduced, including: conducting polymers,[7,8] carbon nanotubes,[9,10] graphene,[11,12] and metallic nanowires.[13,14]

Of all the alternative TCFs, silver nanowire (AgNW) transparent electrodes are considered amongst the most promising for use in PSCs by virtue of their excellent opto-electrical properties and high flexibility.[13–17] There are, however, still several issues that prevent its practical application. Firstly, the rough surface topology of AgNW films presents a major problem in terms of creating short circuits in organic optoelectronic devices. Secondly, the force of adhesion between AgNWs and various substrates tends to be quite weak, thereby limiting the conductivity and stability of the AgNW electrode. Thirdly, AgNWs have a tendency to melt or oxidize during thermal annealing in air, which again degrades the performance of the AgNW electrode. Methods developed to overcome these problems include coating the electrodes with a layer of poly(3,4-ethylene dioxythiophene)-polystyrene sulfonic acid (PEDOT:PSS), or using graphene and metal oxides to smooth the surface of the AgNW films and improve their stability;[16–21] but such layers tend to be easily damaged by common solvents such as water, ethanol or organic reagents. Other methods to improve AgNW adhesion include: the application of high pressure,[22–24] *in situ* polymerization,[25] surface encapsulation[26] and high-intensity pulsed light sintering.[27] Such methods, however, tend to be energy intensive or time-consuming when rapid production is required. Embedding AgNWs into polymer films is a promising way to smooth rough surface and improve adhesion of AgNW films. Polymers such as polymethacrylate,[28] polyvinyl alcohol[29] and poly(dimethylsiloxane)[30] have been applied to composite with AgNWs, which exhibit excellent opto-electrical properties and flexibility. But they suffer either high-temperature treatment or being dissolution in the solvent.

The abrasion performance of modified AgNW films, an important parameter in commercial applications, is something which has been seldom mentioned in the past. This is a significant oversight, in that a TCF with poor abrasion performance can be more easily damaged either before or during device processing, thus leading to a reduced production yield and lower reliability of the optoelectronic devices. More importantly, the properties of modified AgNW films at ultralow temperatures has been largely ignored for a long time, yet has a

State Key Laboratory of Luminescence and Applications, Changchun Institute of Optics, Fine Mechanics and Physics, Chinese Academy of Sciences, Changchun 130033, China. E-mail: liuxy@ciomp.ac.cn; Tel: +86 431 86176341

† Electronic supplementary information (ESI) available: Additional transmittance spectra, sheet resistance of ITO under repeated bending, defined bending angle, AFM images, and experimental photos. See DOI: 10.1039/c5ra00403a

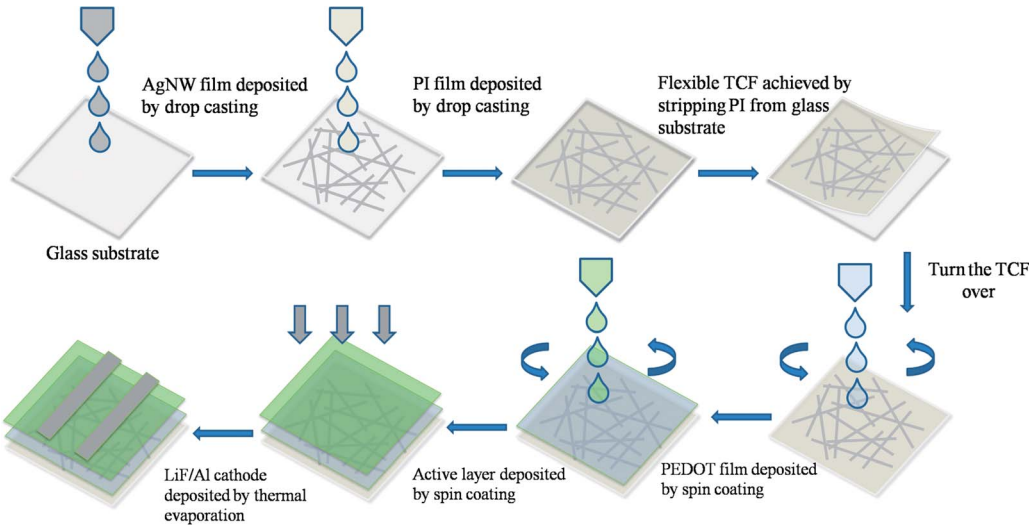

Fig. 1 Fabrication of a flexible PSC based on a PI/AgNW composite film.

significant bearing on the use of optoelectronic devices under extreme environmental conditions.

Herein, we propose a flexible transparent conductive substrate based on an AgNW and polyimide (PI) composite structure, and investigate its durability at high and ultra-low temperatures, and with exposure to air and chemical solvents. Mechanical properties such as flexibility, adhesion and abrasion performance are also investigated. The performance of a flexible PSC based on this new film is compared against a traditional ITO-based device, and the flexible PSC also works well at high and ultra-low temperatures.

Experimental section

Fabrication of PI/AgNW composite transparent electrodes

The method of fabrication used to produce the flexible polymer solar cell based on PI/AgNW composite film is shown in Fig. 1. AgNWs (Bule nano, 50–60 nm) dispersed in an anhydrous ethanol solution were dropped onto pre-cleaned K9 glass, which was then placed on a hot plate to remove the solvent. After annealing at 60 °C for 10 min, a PI film was deposited on the substrate with AgNWs by drop casting, with the film then heated to 60 °C for 30 min. The resulting composite film, consisting of PI impregnated with AgNWs, was then carefully stripped from the glass substrate.

Fabrication of polymer solar cells

Devices were fabricated based on either PI/AgNW or PET/ITO (40 Ω sq^{-1}) substrates. PEDOT:PSS layers (Baytron P AI 4083, 30 nm) were then spin-coated onto these substrates and baked on a hot plate at 120 °C for 10 min. The active layers of the polymer solar cells, which were based on a poly[4,8-bis-(2-ethylhexyloxy)-benzo[1,2-*b*:4,5-*b*′]dithiophene-2,6-diyl-*alt*-4-(2-ethylhexyloxy)-thieno[3,4-*b*] thiophene-2,6-diyl] (PBDTTT-C, Solarmer): [6,6]-phenyl C71-butyric acid methyl ester (PC70BM, American Dye) blend (1 : 1.5 weight ratio, 90 nm thick) with 3% 1,8-diodooctane (Sigma Aldrich) were then spin-coated onto the substrates from a dichlorobenzene solution in a glove box. Finally, LiF (1 nm) and Al (100 nm) were thermally deposited at a pressure of approximately 4×10^{-4} Pa. The active area of the solar cells was 0.12 cm^2. All measurements were performed in air without encapsulation.

Film and device characterization

The surface resistance was measured using the four-point probe method with a surface resistivity meter. Optical transmittance spectra were obtained using a Shimadzu UV-3101PC spectrophotometer. Surface images of the composite films were obtained by scanning electron microscopy (SEM, Hitachi S-4800), and atomic force microscopy (AFM) measurements were performed with a Shimadzu SPA-9700. The thickness of each film was measured using an Ambios XP-1 surface profiler. The high and ultra-low temperature measurements were carried out by a hot plate and a plate cooling by liquid nitrogen, respectively. The current density and voltage (*J*–*V*) characteristics of the polymer PV cells were measured using a computer-controlled Keithley 2611 source meter under AM 1.5G illumination from a calibrated solar simulator with an irradiation intensity of 100 mW cm^{-2}. External quantum efficiency (EQE) measurements were performed using a lock-in amplifier at a chopping frequency of 20 Hz, with illumination provided by a monochromatic Xe lamp. All measurements were performed in air under ambient conditions.

Results and discussion

The surface topology of the composite films produced was analyzed by SEM and AFM, the results of which are shown in Fig. 2. It can be seen from Fig. 2a and c that the AgNW networks are well embedded at the surface of the composite film. Fig. 2b shows the AFM height image of the AgNW on a glass substrate, revealing that the root-mean-square (RMS) roughness of the AgNW networks on a flat substrate is 32.3 nm and its peak-to-peak range is about 236 nm. This height of the AgNW film

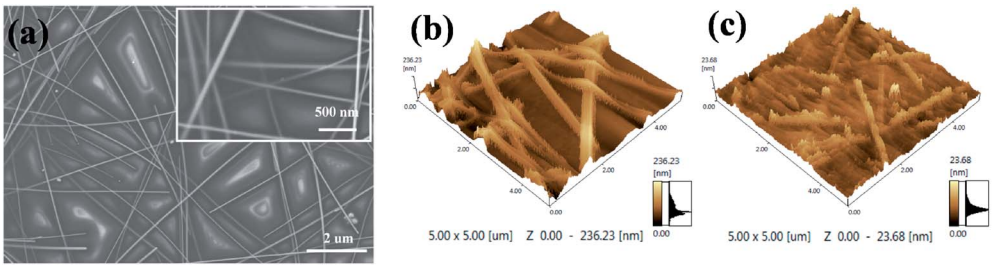

Fig. 2 (a) SEM images of a flexible PI/AgNW composite film. AFM height images of (b) glass/AgNWs and (c) PI/AgNW composite film.

can cause device short circuits, and is attributed to the AgNW network being arranged through a stacking of wires. In contrast, the PI/AgNW composite film (Fig. 2c) has an extremely smooth surface topology, giving a RMS of 2.3 nm and a peak-to-peak range of 24 nm.

The conductivity and optical transparency of the flexible composite films are determined by their AgNW density, which can be readily controlled by either the concentration of the AgNW dispersion or the coating process used. Fig. 3a shows the transmittance of composite films with different sheet resistances, with the transmittance of ITO on a plastic substrate also shown for comparison. This demonstrates that the transmittance of the composite film decreases as the sheet resistance is reduced; however, in order to compare individual films with different sheet resistances, a figure of merit (Φ_{TC}) needs to be introduced to rank the quality of the transparent electrodes. This has been defined by Haacke as $\Phi_{TC} = T^{10}/R_{sh}$,[31] where T is the transmittance, and R_{sh} is the sheet resistance. Values of Φ_{TC} obtained in this way for the flexible PI/AgNW composite films at a wavelength of 600 nm are provided in Table 1, and presented in Fig. 3b as a function of the sheet resistance. We see from this that although the sheet resistance can be reduced by increasing the AgNW coverage, this also results in a substantial decline in the optical transparency of the film. As a result, the Φ_{TC} value tends to exhibit significant fluctuation, with a maximum value of 7.8×10^{-3} Ω^{-1} obtained with a transmittance of 83% and a sheet resistance of 20 Ω sq^{-1}. As a comparison, the Φ_{TC} value of a PET/ITO electrode (6.1×10^{-3} Ω^{-1}) calculated using the same method is notably lower, suggesting that the PI/AgNW composite film with a sheet resistance of 20 Ω sq^{-1} has definite potential to replace ITO as transparent electrode in flexible devices.

Table 1 Values of the transmittance at 600 nm, sheet resistance, and figure of merit of the flexible TCFs

Film	Transmittance at 600 nm (%)	Sheet resistance (Ω sq^{-1})	Figure of merit (10^{-3} Ω^{-1})
PI/AgNW	90.9	190	0.1
	87.3	70	2.2
	83.0	20	7.8
	66.8	8	3.7
	46.2	4	2.0
PET/ITO	86.9	40	6.1

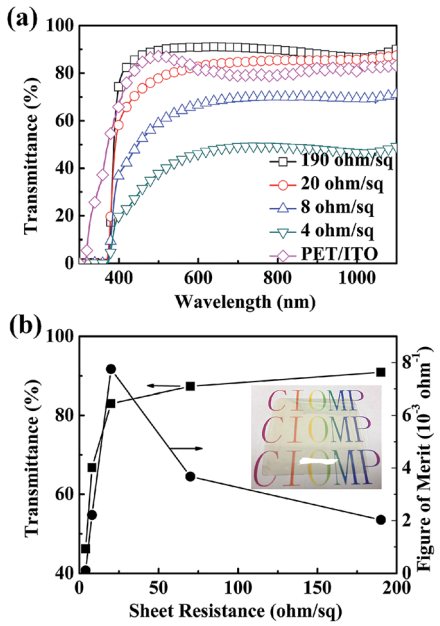

Fig. 3 (a) Transmittance spectra at different sheet resistances (the transmittance of a PET/ITO electrode is shown for comparison). (b) Transmittance (600 nm) and figure of merit values as a function of sheet resistance. The inset shows a photo of the flexible TCF (70 mm × 70 mm, ~20 Ω $\square^{-1}$).

The thermal, environmental and chemical stability of TCFs is an important consideration in flexible device production, with Fig. 4a showing the relative change in the sheet resistance of a PI/AgNW composite film when annealed at different temperatures in air for 30 min. Note that the sheet resistance remains almost unchanged at temperatures between −150 and 150 °C, but decreases from 20 Ω sq^{-1} at 60 °C to 18 and 17 Ω sq^{-1} at 200 and 250 °C, respectively. This is considered to be the result of the composite structure preventing melting and coalescence of the film during thermal annealing, thereby ensuring better contact between the AgNWs[32] and explaining the reduced relative change in sheet resistance at higher temperatures seen in Fig. 4a.

The transmittance spectra of the PI/AgNW composite films were mostly consistent after annealing at different temperatures (Fig. S1†), with Fig. 4b showing the relative change in the sheet resistance of an AgNW film on glass and a PI/AgNW composite film as a function of exposure time in air. This reveals that the sheet resistance of the AgNW film increases by over 160% after exposure to air for 528 hours, which is

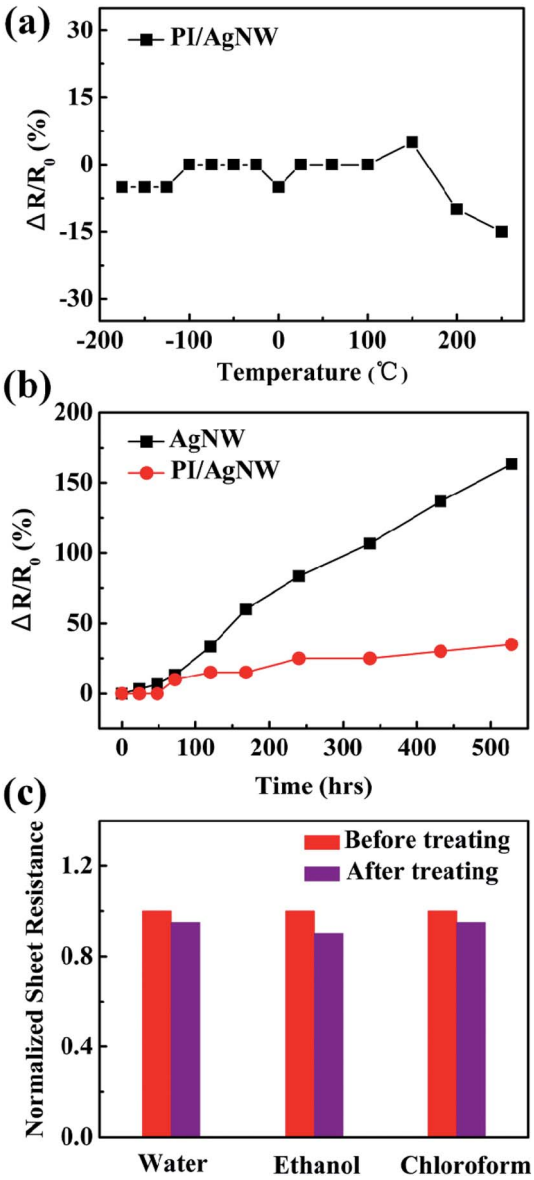

Fig. 4 (a) Relative change in sheet resistance after annealing at different temperatures for 30 min. (b) Relative change in sheet resistance as a function of exposure time in air (the results for an AgNW film on a glass substrate are shown for comparison). (c) Normalized sheet resistance before and after exposure to common solvents. All measurements were carried out in air.

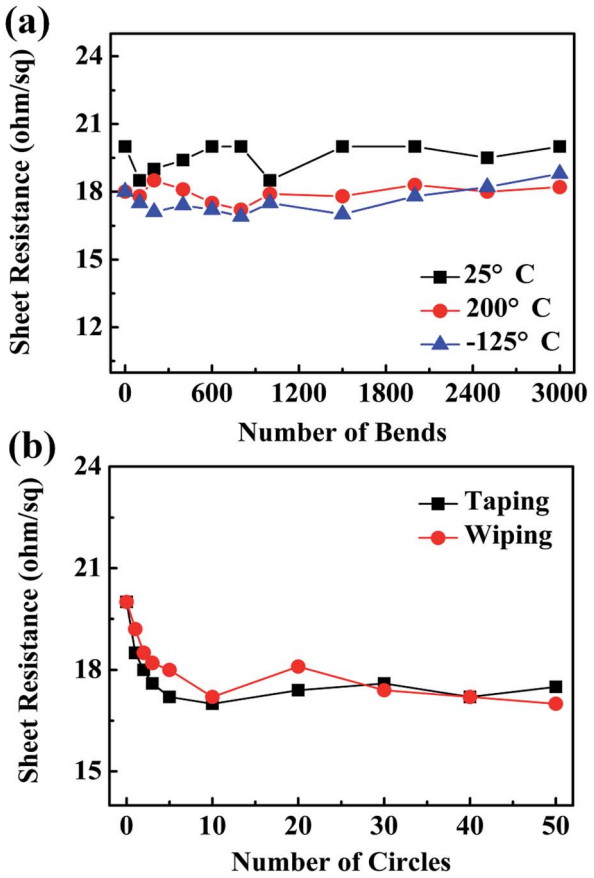

Fig. 5 (a) Sheet resistance after repeated bending to ~90° at different temperatures (the bending angle is shown in Fig. S3†). (b) Sheet resistance after repeated taping and wiping.

consistent with previous reports of AgNWs oxidizing in air.[27,33] However, the sheet resistance of the PI/AgNW composite film increases by only 35% (from 20 Ω sq^{-1} to 27 Ω sq^{-1}), indicating that the composite structure prevents oxidation of the AgNWs.

Fig. 4c depicts the change in the sheet resistance of the PI/AgNW composite film before and after exposure to common solvents, identifying a slight decrease in resistance with cleaning by water, ethanol and chloroform. This phenomenon can be attributed to an improved NW–NW network created by the solvent removal of disconnected AgNWs from the film surface.

Given the importance of a TCF's flexibility, adhesion and abrasion resistance in determining its suitability for use in flexible optoelectronic devices, the sheet resistance of the PI/AgNW films was tested after repeated bending at different temperatures. From the results shown in Fig. 5a, it is apparent that there is little change in sheet resistance despite 3000 bending cycles, even at different temperatures (25, 200 and −125 °C), which is clearly indicative of excellent durability. Furthermore, the flexibility of the PI/AgNW composite film is much better than that of PET/ITO electrodes (Fig. S2†). The mechanical adhesion and abrasion performance of the PI/AgNW composite film was also studied, as shown in Fig. 5b, revealing a slight decrease in sheet resistance from ~20 to ~17.5 Ω sq^{-1} after applying and removing an adhesive tape fifty times. The sheet resistance also decreased slightly from ~20 Ω sq^{-1} to ~17 Ω sq^{-1} after wiping with a cotton swab fifty times. It is considered that in either instance disconnected AgNWs on the composite film surface are removed, resulting in an improved NW–NW network and reduced sheet resistance (Fig. S4†). In comparison, when identical tests were performed on an AgNW film deposited on a glass substrate, virtually all of the AgNW network was removed.

PSCs based on a low band gap conjugated polymer PBDTTT-C and $PC_{70}BM$ were prepared on a PI/AgNW composite film to further test the film's properties. Fig. 6a shows the *J*–*V* characteristics of these PV cells under 100 mW cm^{-2} AM 1.5G

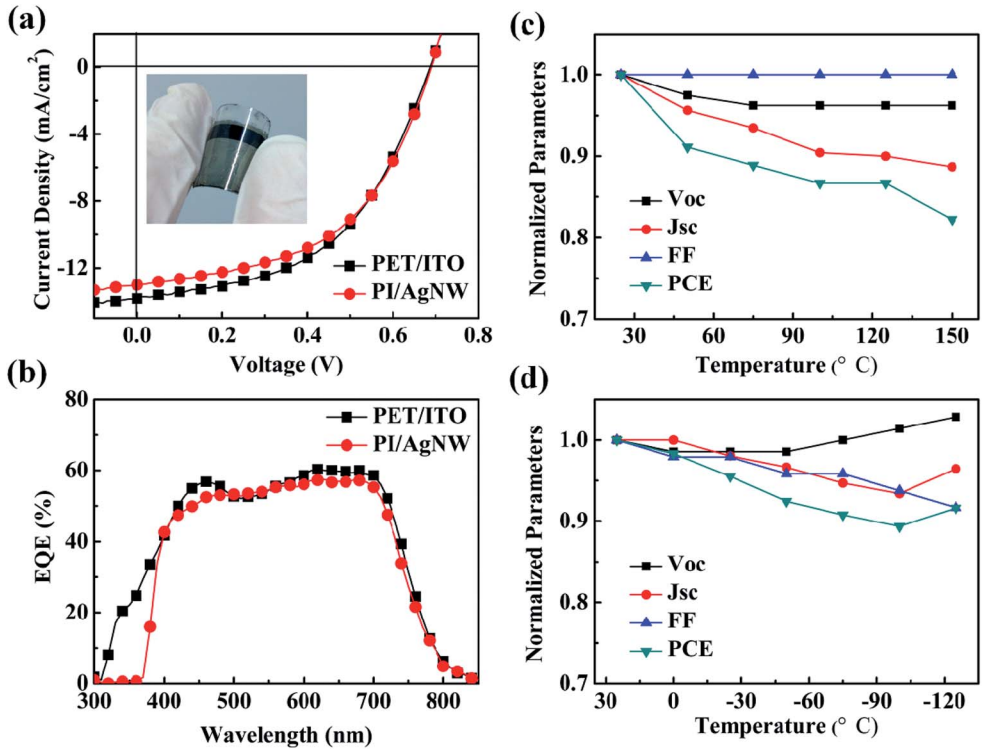

Fig. 6 (a) J–V characteristics and (b) EQE spectra (results for a PET/ITO electrode are also shown for comparison). Normalized parameters of PI/AgNW based device during (c) heating and (d) cooling.

Table 2 Performance of polymer PV cells based on different substrates

Device	V_{OC} (V)	J_{SC} (mA cm^{-2})	Calculated J_{SC} (mA cm^{-2})	FF	PCE (%)	R_s (Ω cm^2)
PET/ITO	0.69 ± 0.01	13.84 ± 0.25	13.45	0.50 ± 0.01	4.76 ± 0.24	10.4
PI/AgNW	0.69 ± 0.01	13.01 ± 0.25	12.67	0.51 ± 0.01	4.58 ± 0.25	4.4

illumination, with the results obtained from a conventional PET/ITO-based cell also shown for comparison. The detailed parameters for each of these cells are summarized in Table 2. With the reference device using PET/ITO as the transparent electrode, a PCE of 4.76% was obtained with a short-circuit current density (J_{SC}) of 13.84 mA cm^{-2}, a V_{OC} of 0.69 V and a FF of 0.50. The PI/AgNW device, on the other hand, showed quite promising performance with a V_{OC} of 0.69 V, a J_{SC} of 13.01 mA cm^{-2}, a FF of 0.51, and a PCE of 4.58%. The lower PCE is attributed to the smaller J_{SC} value caused by the PI film limiting the absorption of the active layer, which was confirmed by the EQE spectra of devices based on different substrates (Fig. 6b). The J_{SC} values calculated from the EQE spectra are also listed in Table 2, and are almost consistent with the measured values. The series resistance (R_s) values of the two devices, as calculated from the J–V curves under light, are also shown in Table 2. Compared with the PET/ITO devices (10.4 Ω cm^2), those based on the composite film show a lower R_s of 4.4 Ω cm^2 that is most likely due to their lower sheet resistance, and which results in a higher FF. Device performance under different temperatures was also measured (Fig. 6c and d), revealing that the PCEs of the flexible PSCs decrease with heating or cooling; ~82 and ~90% of its initial PCE achieved at temperatures of 150 and −125 °C, respectively.

The stabilities of the flexible PSCs under different temperatures have also been studied. Fig. 7a–c shows the normalized device parameters as a function of exposure time in air at different temperatures. The PCEs of the flexible PSCs decrease as the exposure time increasing, 33, 57 and 72% of its initial PCE achieved at temperatures of 100, 28 (room temperature) and −100 °C for 30 min, respectively. Comparing with the device stabilities at room temperature, the flexible PSC shows better stabilities at ultra-low temperature of −100 °C and worse stabilities at high temperature of 100 °C. The variation in Fig. 6c and d was consistent to that seen in Fig. 7, which confirmed that devices under heating process degenerated faster than that under cooling process. The reason for the fast degeneration of the device under 100 °C for 30 min may be attributed to the macrophase separation and interface or electrode degradation under heating in air without encapsulation.[34,35] Nevertheless, it is clear that polymer solar cells

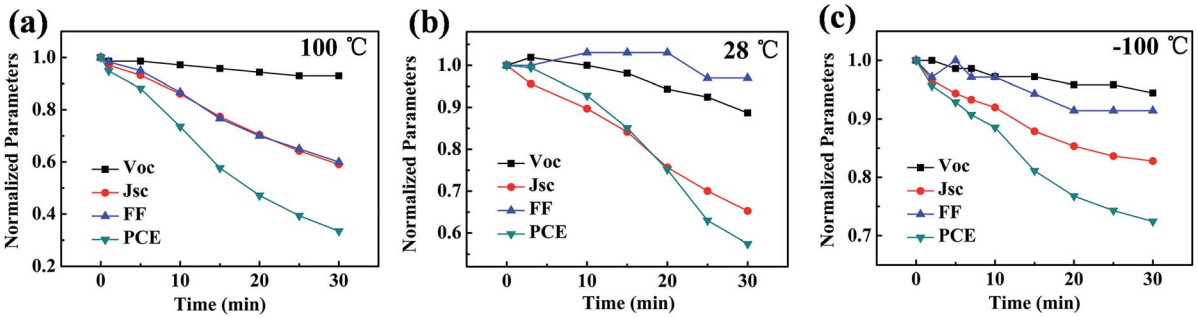

Fig. 7 Normalized parameters of a flexible PSC based on a PI/AgNW composite film as a function of its exposure to air at different temperatures of (a) 100, (b) 28 (room temperature) and (c) −100 °C, respectively.

based on a PI/AgNW composite film are quite stable under a range of applied temperatures.

Conclusions

In conclusion, a high and ultra-low temperature resistant flexible polymer solar cell based on a PI/AgNW composite transparent electrode has been proposed. Through this study, it has been shown that the PI/AgNW composite TCF can achieve a high transmittance of 83%, combined with a low sheet resistance of 20 Ω sq^{-1}. Such films also possess excellent mechanical properties in terms of flexibility, adhesion and abrasion resistance, as well as excellent thermal, environmental and chemical stability. Furthermore, the PCE of PSCs based on this composite film (4.58%) is comparable to that of devices fabricated on conventional flexible ITO electrodes. The flexible PSC also shows stable properties under ultralow and high temperatures which confirms the viability of using PI/AgNW composite TCFs as a transparent electrode in flexible optoelectronic devices.

Acknowledgements

The authors acknowledge financial support from the CAS Innovation Program, the National Natural Science Foundation of China no. 61106057 and the Jilin Province Science and Technology Research Project no. 20140520119JH, and project supported by State Key Laboratory of Luminescence and Applications.

Notes and references

1 G. Li, V. Shrotriya, J. S. Huang, Y. Yao, T. Moriarty, K. Emery and Y. Yang, *Nat. Mater.*, 2005, **4**, 864.
2 Y. Kim, S. Cook, S. M. Tuladhar, S. A. Choulis, J. Nelson, J. R. Durrant, D. D. C. Bradley, M. Giles, I. Mcculloch, C. S. Ha and M. Ree, *Nat. Mater.*, 2006, **5**, 197.
3 J. Peet, J. Y. Kim, N. E. Coates, W. L. Ma, D. Moses, A. J. Heeger and G. C. Bazan, *Nat. Mater.*, 2007, **6**, 497.
4 S. R. Forrest, *Nature*, 2004, **428**, 911.
5 B. H. Lee, S. H. Park, H. Back and K. Lee, *Adv. Funct. Mater.*, 2011, **21**, 487.
6 R. B. H. Tahar, T. Ban, Y. Ohya and Y. Takahashi, *J. Appl. Phys.*, 1998, **83**, 2631.
7 S. Kirchmeye and K. Reuter, *J. Mater. Chem.*, 2005, **15**, 2077.
8 Y. H. Ha, N. Nikolov, S. K. Pollack, J. Mastrangelo, B. D. Martin and R. Shashidhar, *Adv. Funct. Mater.*, 2004, **14**, 615.
9 Z. C. Wu, Z. H. Chen, X. Du, J. M. Logan, J. Sippel, M. Nikolou, K. Kamaras, J. R. Reynolds, D. B. Tanner, A. F. Hebard and A. G. Rinzler, *Science*, 2004, **305**, 1273.
10 R. C. Tenent, T. M. Barnes, J. D. Bergeson, A. J. Ferguson, B. To, L. M. Gedvilas, M. J. Heben and J. L. Blackburn, *Adv. Mater.*, 2009, **21**, 3210.
11 Z. Yin, S. Sun, T. Salim, S. Wu, X. Huang, Q. He and Y. M. Lam, *ACS Nano*, 2010, **4**, 5263.
12 J. B. Wu, M. Agrawal, H. A. Becerril, Z. N. Bao, Z. F. Liu, Y. S. Chen and P. Peumans, *ACS Nano*, 2010, **4**, 43.
13 J. Y. Lee, S. T. Connor, Y. Cui and P. Peumans, *Nano Lett.*, 2008, **8**, 689.
14 A. R. Rathmell, S. M. Bergin, Y. L. Hua, Z. Y. Li and B. J. Wiley, *Adv. Mater.*, 2010, **22**, 3558.
15 H.-G. Im, J. Jin, J.-H. Ko, J. Lee, J. Y. Lee and B.-S. Bae, *Nanoscale*, 2014, **6**, 711.
16 F. Nickel, T. Haas, E. Wegner, D. Bahroa, S. Salehina, O. Kraft, P. A. Gruber and A. Colsmann, *Sol. Energy Mater. Sol. Cells*, 2014, **130**, 317.
17 D.-S. Leem, A. Edwards, M. Faist, J. Nelson, D. D. C. Bradley and J. C. de Mello, *Adv. Mater.*, 2011, **23**, 4371.
18 J. Krantz, M. Richter, S. Spallek, E. Spiecker and C. J. Brabec, *Adv. Funct. Mater.*, 2011, **21**, 4784.
19 D. Lee, H. Lee, Y. Ahn, Y. Jeong, D.-Y. Lee and Y. Lee, *Nanoscale*, 2013, **5**, 7750.
20 M. Song, D. S. You, K. Lim, S. Park, S. Jung, C. S. Kim, D.-H. Kim, D.-G. Kim, J.-K. Kim, J. Park, Y.-C. l. Kang, J. Heo, S.-H. Jin, J. H. Park and J.-W. Kang, *Adv. Funct. Mater.*, 2013, **23**, 4177.
21 M.-S. Lee, K. Lee, S.-Y. Kim, H. Lee, J. Park, K.-H. Choi, H.-K. Kim, D.-G. Kim, D.-Y. Lee, S. Nam and J.-U. Park, *Nano Lett.*, 2013, **13**, 2814.
22 A. R. Madaria, A. Kumar, F. N. Ishikawa and C. Zhou, *Nano Res.*, 2010, **3**, 564.
23 W. Gaynor, J. Y. Lee and P. Peumans, *ACS Nano*, 2010, **4**, 30.
24 W. Gaynor, G. F. Burkhard, M. D. McGehee and P. Peumans, *Adv. Mater.*, 2011, **23**, 2905.

25 Z. Yu, Q. Zhang, L. Li, Q. Chen, X. Niu, J. Liu and Q. Pei, *Adv. Mater.*, 2011, **23**, 664.
26 L. Hu, H. S. Kim, J. Y. Lee, P. Peumans and Y. Cui, *ACS Nano*, 2010, **4**, 2955.
27 J. Jiu, M. Nogi, T. Sugahara, T. Tokuno, T. Araki, N. Komoda, K. Suganuma, H. Uchida and K. Shinozaki, *J. Mater. Chem.*, 2012, **22**, 23561.
28 Z. Yu, L. Li, Q. Zhang, W. Hu and Q. Pei, *Adv. Mater.*, 2011, **23**, 4453.
29 X. Y. Zeng, Q. K. Zhang, R. M. Yu and C. Z. Lu, *Adv. Mater.*, 2010, **22**, 4484.
30 F. Xu and Y. Zhu, *Adv. Mater.*, 2012, **24**, 5117.
31 G. Haacke, *J. Appl. Phys.*, 1976, **47**, 4086.
32 J. Jin, J. Lee, S. Jeong, S. C. Yang, J.-H. Ko, H.-G. Im, S.-W. Baek, J.-Y. Lee and B.-S. Bae, *Energy Environ. Sci.*, 2013, **6**, 1811.
33 S. De and J. N. Coleman, *MRS Bull.*, 2011, **36**, 774.
34 T. S. Quintana, T. Heumüller, W. R. Mateker, D. E. Orozco, R. Cheacharoen, S. Sweetnam, C. J. Brabec and M. D. McGehee, *Adv. Funct. Mater.*, 2014, **24**, 3978.
35 D. Qian, Q. Xu, X. Hou, F. Wang, J. Hou and Z. Tan, *J. Polym. Sci., Part A: Polym. Chem.*, 2013, **51**, 3123.